Nuclear pore density controls heterochromatin reorganization during senescence

Nuclear pore density controls heterochromatin reorganization during senescence

Charlene Boumendil[1], Priya Hari[2], Karl C. F. Olsen[1], Juan Carlos Acosta[2*], Wendy A. Bickmore[1*]

[1]MRC Human Genetics Unit, Institute of Genetics and Molecular Medicine, University of Edinburgh, Edinburgh EH4 2XU

[2]Cancer Research UK Edinburgh Centre, Institute of Genetics and Molecular Medicine, University of Edinburgh, Edinburgh EH4 2XU

[*]correspondence to WAB, MRC Human Genetics Unit, IGMM, University of Edinburgh, Crewe Road South, Edinburgh EH4 2XU. Wendy.Bickmore@igmm.ed.ac.uk

or JCA, Cancer Research UK Edinburgh Centre, IGMM, University of Edinburgh, Crewe Road South, Edinburgh EH4 2XU. Juan-Carlos.Acosta@igmm.ed.ac.uk

Abstract

During oncogene induced senescence (OIS) heterochromatin is lost from the nuclear periphery and forms internal senescence associated heterochromatin foci (SAHF). We show that an increased nuclear pore density during OIS is responsible for SAHF formation. In particular, the nucleoporin TPR is necessary for both formation and maintenance of SAHF. Loss of SAHF does not affect cell-cycle arrest but abrogates the senescence associated secretory phenotype – a programme of inflammatory cytokine gene activation. Our results uncover a previously unknown role of nuclear pores in heterochromatin re-organization in mammalian nuclei and demonstrate the importance of heterochromatin organisation for a specific gene activation programme.

Introduction

3D genome organization is governed by a combination of polymer biophysics and biochemical interactions, including local chromatin compaction, long-range chromatin interactions and interactions with nucleus structures. One such structure is the nuclear lamina (NL), which coats the inner nuclear membrane and is composed of lamins and membrane associated proteins, such as LBR. Electron

microscopy (E.M.) reveals large blocks of heterochromatin associated with the nuclear periphery (Capelson and Hetzer, 2009), and mapping genome interactions with laminB1 identifies > 1000 lamina-associated domains (LADs). LADs are associated with heterochromatic histone marks (H3K27me3 or H3K9me3) (Guelen et al., 2008). Altered NL composition in the photoreceptors of nocturnal mammals leads to the loss of heterochromatin from the nuclear periphery and its accumulation at the centre of the nucleus (Solovei et al., 2013).

Another situation in which there is a dramatic reorganisation of heterochromatin is in oncogene-induced senescence (OIS) - a cell cycle arrest program triggered by oncogenic signalling. OIS cells undergo striking chromatin reorganization, with loss of heterochromatin and constitutive LADs (Lenain et al., 2017) from the nuclear periphery and the appearance of internal senescence-associated heterochromatin foci (SAHF). SAHF appear consecutive to cell cycle arrest and are not observed in non-transformed replicating cells (Narita et al. 2003). SAHF formation results from a reorganization of pre-existing heterochromatin –regions decorated with H3K9me3, H3K27me3, MacroH2a and HP1α,β,γ - rather than de novo heterochromatin formation on new genomic regions (Narita et al., 2003; Zhang et al., 2005; Chandra et al., 2012; Sadaie et al., 2013). Known factors implicated in SAHF formation include; activation of the pRB pathway (Narita et al., 2003), certain chromatin-associated non-histone proteins (Narita et al., 2006) and the histone chaperones HIRA and Asf1a (Zhang et al., 2005, 2007). The NL has also been implicated in SAHF formation: LaminB1 and Lamin B receptor (LBR) expression are decreased in OIS and their experimental depletion can facilitate, but is not sufficient for, SAHF formation (Sadaie et al., 2013; Lukášová et al., 2017).

The nuclear envelope is perforated by nuclear pores that control transport between the cytoplasm and nucleus. The nuclear pore complex (NPC) is a large transmembrane complex, consisting of about 30 proteins called nucleoporins (Fig. 1A) (Kim et al., 2018). In contrast to the adjacent NL, E.M. and super-resolution light microscopy show that the nuclear area underneath nuclear pores is devoid of heterochromatin (Schermelleh et al., 2008; Capelson and Hetzer, 2009) and nuclear pore density in different neurons and glial cell types from the rat cerebellar cortex anticorrelates with compact chromatin (Garcia-Segura et al. 1989). The nucleoporin TPR has been shown to be responsible for heterochromatin exclusion zones at NPCs (Krull et al., 2010).

The composition and density of NPCs changes during differentiation and tumorigenesis (D'Angelo et al., 2012;; Raices and D'Angelo, 2012; Sellés et al., 2017; Rodriguez-Bravo et al., 2018). We therefore

hypothesized that NPCs could contribute to global chromatin organization and that, specifically, heterochromatin organization could result from a balance of forces attracting heterochromatin to the NL and forces repelling it away from the NPCs (Fig. 1B). In support of this hypothesis, here we show that nuclear pore density increases during OIS and that this increase is necessary for heterochromatin reorganization into SAHF. We identify TPR as a key player in this reorganization. Furthermore, we demonstrate the functional consequences of heterochromatin reorganization in OIS for the programmed activation of inflammatory cytokine gene expression – the senescence-associated secretory phenotype (SASP).

Results and discussion

Nuclear pore density increases during OIS

To assess the role of NPCs in SAHF formation during OIS, we induced the activity of oncogenic Ras (RAS^{G12D}) by addition of 4-hydroxy-tamoxifen (4HT) in human IMR90 cells, leading to OIS, activation of p53 and p16 and expression of SASP proteins (Acosta et al., 2013) (Fig. 1C; Fig. S1A). Nuclear pores disassemble upon entry into mitosis but are very stable during interphase (Daigle et al., 2001; Dultz and Ellenberg, 2010). In quiescent cells nuclear pore density is stabilised by down-regulation of nucleoporin mRNAs (D'Angelo et al., 2009). However, expression profiling in OIS cells (ER:Ras) showed that, compared with control ER:STOP (STOP codon) cells, nucleoporin mRNA levels are unchanged during senescence (Fig. S1B). Nucleoporin protein accumulation in senescent cells was confirmed by immunoblotting for POM121 – an integral membrane protein of the NPC central ring (Funakoshi et al., 2011) and TPR – a large coiled-coil protein of the nuclear basket (Cordes et al., 1998) (Fig. 1A, D). Immunofluorescence and structured illuminated microscopy (SIM) (Schermelleh et al., 2008) showed that increased nucleoporin levels during OIS results in an increased nuclear pore density (Fig. 1E-G).

Decreasing nuclear pore density leads to loss of SAHF formation

To assess whether the increased nuclear pore density is responsible for heterochromatin reorganization into SAHF, we used siRNAs to deplete POM121 (Fig. S2A) during the entire course of OIS induction (Fig. 2A). As expected, since POM121 is required for NPC assembly during interphase (Dultz and Ellenberg, 2010; Funakoshi et al., 2011), this led to a decrease in nuclear pore density (Fig. 2B, C and

Fig. S2B). Consistent with our hypothesis, POM121 depletion resulted in a reduction of OIS cells containing SAHF (Fig. 2D, E).

The nucleoporin TPR is necessary for SAHF formation and maintenance

TPR is the last nucleoporin to be incorporated in new NPCs (Bodoor et al., 1999) through its interaction with NUP153 (Hase and Cordes, 2003) (Fig. 1A). TPR has been shown to establish heterochromatin exclusion zones at nuclear pores (Krull et al. 2010) and to influence HIV integration sites by maintaining an open chromatin architecture near the NPCs (Lelek et al.. 2015).

To determine if it is the increased abundance of TPR at the nuclear periphery of OIS cells, as a result of elevated nuclear pore density, that is responsible for SAHF formation, we depleted TPR during OIS induction (Fig. S3A, B). Contrary to a recent report, TPR depletion did not affect nuclear pore density (McCloskey et al., 2018) (Fig. S3C). However similar to POM121 depletion, TPR depletion led to the loss of SAHF (Fig. 3A, B). We confirmed these results with four independent siRNAs targeting TPR (Fig. S3D-F). We conclude that TPR is necessary for the formation of SAHF during OIS.

The effect of TPR knockdown on heterochromatin re-localization during OIS does not appear to be due to obvious changes in the amount of laminB1 at the nuclear lamina, (Fig S4A).

To assess whether TPR is necessary for maintenance as well as the formation of SAHF, we used a time course to determine when SAHF are formed. The percentage of cells containing SAHF increased gradually after 4HT treatment of ER:Ras cells, reaching a maximum at 6 days (Fig. S4B). We therefore depleted TPR 6 days after 4HT addition, when SAHF have already formed (Fig. 3C). We observed a dramatic reduction of cells containing SAHF two days later (day 8) (Fig. 3D, E). siRNA depletion under these conditions was only partial and we observed loss of SAHF in cells specifically depleted for TPR, whereas SAHF were maintained in cells where knockdown was incomplete (Fig. S4C). In some cells with partial TPR depletion, there was a relocalization of heterochromatin to the nuclear periphery in patches that correspond to sites of TPR-depletion (Fig. 3F), but that still contained nuclear pores as detected by MAB414 staining (Fig 3G). We conclude that exclusion of heterochromatin from the nuclear periphery by TPR is necessary for both the formation and maintenance of SAHF during OIS.

TPR is necessary for the senescence-associated secretory phenotype

SAHF are proposed to be involved in silencing pro-mitotic genes, contributing to stable cell cycle arrest (Narita et al., 2003; Narita et al., 2006; Zhang et al., 2007). However, TPR- depleted OIS cells did not show defective cell-cycle arrest as assayed by BrdU incorporation and activation of p16, p21 and p53 (Fig. S5A-C). This suggests that SAHF are dispensable for cell-cycle arrest, in agreement with the fact that not all senescent cells form SAHF (Kosar et al., 2011). Furthermore SAHF have been shown to be insufficient to maintain cell cycle arrest as inactivation of p53 or ATM in OIS cells leads to senescence escape without SAHF alteration (Di Micco et al., 2011).

An important characteristic of OIS is activation of the senescence associated secretory phenotype (SASP) which is responsible for the non–cell autonomous effects of senescence. SASP consists of the expression and secretion of cytokines, chemokines, extracellular matrix proteases, growth factors and other signalling molecules. SASP is a tumour suppressive mechanism which reinforces cell cycle arrest and leads to paracrine senescence but can also promote tumour progression in premalignant lesions (Coppé et al., 2010; Acosta et al., 2013). Strikingly, in the absence of SAHF after TPR depletion, we observed a complete loss of the SASP as exemplified by lack of IL1α, IL1β, IL6 and IL8 mRNA and protein (Fig 4A-C, Fig. S5D, E). SAHF and SASP loss upon TPR depletion does not seem to be due to a general defect in nuclear transport as we detected NFκB nuclear import upon induction of paracrine senescence (Acosta et al., 2008; Chien et al., 2011; Acosta et al., 2013) (Fig. S6A- C).

Similarly to some other nucleoporins, a fraction of TPR is present in the nucleoplasm as well as at nuclear pores (Frosst et al., 2002). To assess whether it is the increase in nuclear pore density in OIS – and consequent increased TPR abundance at the nuclear periphery - that is necessary for SASP or whether TPR has an independent role, we assessed SASP upon depletion of POM121 which is only present within the NPC. Decreased nuclear pore density upon POM121 depletion did not affect cell-cycle arrest (Fig. S7A), but the SASP was impaired (Fig. S7B-D).

The nuclear pore basket nucleoporin NUP153 (Fig. 1A) is necessary for the association of TPR with the NPC (Hase and Cordes 2003). To further confirm that the role of TPR in SAHF formation and SASP depends on its presence at the NPC rather than in the nucleoplasm, we depleted NUP153 (Fig. S8A), NPC density was unchanged (Fig. S8B), but consistent with the role of NUP153 in TPR-nuclear basket association, TPR-containing NPC density decreased upon NUP153 depletion (Fig. S8C).

Concomitantly, the percentage of SAHF containing cells decreased (Fig. S8D, E) and the SASP was lost (Fig. S8F). We conclude that it is TPR association with NPC that is necessary for SAHF formation and SASP activation in OIS.

Chromatin reorganization controls the SASP

Our results suggest that heterochromatin reorganization is necessary for SASP during OIS. To exclude that nuclear pores regulate SASP through another independent mechanism, we used a different means to deplete SAHF. The histone chaperone ASF1a is required for SAHF formation (Zhang et al., 2005, 2007) and indeed its depletion led to a loss of SAHF in ER-Ras cells (Fig. 5A-C). ASF1a depletion did not affect nuclear pore density (Fig. 5D), but as for TPR and POM121 depletion, there is a dramatic loss of the SASP upon ASF1a depletion in ER-Ras cells (Fig. 5E). Whilst we cannot completely rule out that intact nuclear pores are needed for SASP activation independent of chromatin reorganization, this result supports the hypothesis that heterochromatin reorganization is necessary for the SASP.

Our data suggest that an increase in nuclear pore density is responsible for the eviction of heterochromatin from the nuclear periphery by TPR and the consequent formation of SAHF in OIS. Similar mechanisms could be conserved in other types of senescence as nuclear pore density is also increased in replicative senescence (Maeshima et al. 2006). Chromatin organisation relative to the nuclear periphery has generally been considered from the point of view of interactions between (hetero)chromatin and components of the nuclear lamina. Here we demonstrate that the repulsion of heterochromatin by nuclear pores is another important principle of nuclear organisation and it will be interesting to establish whether the modulation of nuclear pore density also influences the 3D organisation of the genome during development.

Methods

Cell culture

IMR90 cells were infected with pLNC-ER:RAS and pLXS-ER:Stop retroviral vectors to produce ER-RAS and ER-Stop cells respectively (Acosta et al., 2013). Ras translocation to the nucleus was induced by addition of 4-hydroxy-tamoxifen (4HT) (Sigma) diluted in DMSO to 100 nM. 4HT containing-medium was changed every 3 days.

SiRNA transfection

$2x10^5$ IMR90, ER-STOP and ER-Ras cells were transfected using Dharmafect transfection reagent (Dharmacon) with a 30 nM final concentration of predesigned siRNAs (Dharmacon, Table S1).

RNA expression analysis

mRNA expression profiling was by IonTorrent mRNA sequencing using the Ion AmpliSeq™ Transcriptome Human Gene Expression Kit. 6 biological replicates were analysed and adjusted p-value were calculated by Benjamini and Hochberg (BH) and FDR multiple test correction. Data analysis was performed using Babelomics-5 (http://babelomics.bioinfo.cipf.es).

For individual mRNAs, total RNA was extracted using the RNeasy minikit (QIAGEN) and cDNAs generated using Superscript II (Life technologies). Real-time PCR ws performed on a Lightcycler 480 (Roche) using SYBR Green PCR Master Mix (Roche) using primer listed in Table S3. Expression was normalized to β-actin.

Immunoblotting

$1x10^6$ cells were lysed in RIPA buffer and protein concentration determined using a Pierce BCA protein analysis kit. 15 μg of proteins were run into NuPage 3-8% Tris acetate gels (Invitrogen). After transfer onto nitrocellulose with a iBlot 2 gel transfer device (Thermofisher), immunoblotting was done using antibodies as listed in Table S2.

Immunofluorescence and SAHF measurement

$2x10^5$ cells were seeded and grown on coverslips during senescence induction. Cells were fixed in 4% paraformaldehyde (pFa) for 10 min at room temperature, permeabilized in 0.1% Triton X100 for 10 min, blocked in 1% BSA for 30 min, incubated with primary antibodies diluted in 1% BSA for 1h and with fluorescently labelled secondary antibodies (Life Technologies) for 45 min. Coverslips were counterstained with DAPI and mounted in Vectashield (Vectorlabs).

To detect replicating cells, cells were incubated with 10 μM 5-Bromo-2' – deoxyuridine (BrdU) (Sigma) for 16 h prior to fixation and immunodetection using a BrdU antibody (BD Pharmingene 555627) in the presence of 1 mM $MgCl_2$ and 0.5 U/ul DNaseI (Sigma D4527).

Detection of SASP proteins, tumour suppressors and BrdU positive cells by high content microscopy is

212 described at (Hari and Acosta 2017). The % SAHF positive cells was determined by manual examination
213 of 100-200 DAPI stained cells.
214
215 **Structured Illumination Microscopy (SIM) and measurement of nuclear pores density**
216 The bottom plane of cells was imaged by 3D SIM (Nikon N-SIM) and reconstructed using NIS element
217 software after immunofluorescence with antibodies as indicated in Table S2. 15 nuclei were imaged for
218 each condition and 5 ROI of 100x100 pixels were analyzed/nucleus. Individual nuclear pore complexes
219 in each ROI were counted manually.
220
221 **β-Galactosidase staining**
222 SA-β-Gal staining solution was prepared using 20x KC(100 mM $K_3FE(CN)_6$ and 100 mM $K_4Fe(CN)_6$*$3H_2O$ in PBS), 20x X-Gal solution (ThermoFisher Scientific) diluted to 1x in PBS/1 mM $MgCl_2$ at pH
224 5.5-6. Staining was conducted overnight on glutaraldehyde fixed cells.
225
226 **Statistics**
227 All experiments were performed in a minimum of 3 biological replicates. Error bars are standard error
228 of the mean. P-values were obtained by two sample equal variance, 2 tails t-test.
229
230 **References**

231 Acosta JC, Banito A, Wuestefeld T, Georgilis A, Janich P, Morton JP, Athineos D, Kang T-W,
232 Lasitschka F, Andrulis M, et al. 2013. A complex secretory program orchestrated by the
233 inflammasome controls paracrine senescence. *Nat Cell Biol* **15**: 978–990.

234 Acosta JC, O'Loghlen A, Banito A, Guijarro MV, Augert A, Raguz S, Fumagalli M, Da Costa M, Brown
235 C, Popov N, et al. 2008. Chemokine Signaling via the CXCR2 Receptor Reinforces Senescence. *Cell*
236 **133**: 1006–1018.

237 Bodoor K, Shaikh S, Salina D, Raharjo WH, Bastos R, Lohka M, Burke B. 1999. Sequential
238 recruitment of NPC proteins to the nuclear periphery at the end of mitosis. *J Cell Sci* **112**: 2253-2264.

239 Capelson M, Hetzer MW. 2009. The role of nuclear pores in gene regulation, development and
240 disease. *EMBO Rep* **10**: 697-705.

241 Chandra T, Kirschner K, Thuret J-Y, Pope BD, Ryba T, Newman S, Ahmed K, Samarajiwa SA,
242 Salama R, Carroll T, et al. 2012. Independence of Repressive Histone Marks and Chromatin
243 Compaction during Senescent Heterochromatic Layer Formation. *Mol Cell* **47**: 203–214.

Chien Y, Scuoppo C, Wang X, Fang X, Balgley B, Bolden JE, Premsrirut P, Luo W, Chicas A, Lee CS, et al. 2011. Control of the senescence-associated secretory phenotype by NF-κB promotes senescence and enhances chemosensitivity. *Genes Dev* **25**: 2125–2136.

Coppé J-P, Desprez P-Y, Krtolica A, Campisi J. 2010. The Senescence-Associated Secretory Phenotype: The Dark Side of Tumor Suppression. *Annu Rev Pathol Mech Dis* **5**: 99–118.

Cordes VC, Hase ME, Müller L. 1998. Molecular Segments of Protein Tpr That Confer Nuclear Targeting and Association with the Nuclear Pore Complex. *Exp Cell Res* **245**: 43–56.

Daigle N, Beaudouin J, Hartnell L, Imreh G, Hallberg E, Lippincott-Schwartz J, Ellenberg J. 2001. Nuclear pore complexes form immobile networks and have a very low turnover in live mammalian cells. *J Cell Biol* **154**: 71-84.

D'Angelo MA, Gomez-Cavazos JS, Mei A, Lackner DH, Hetzer MW. 2012. A Change In Nuclear Pore Complex Composition Regulates Cell Differentiation. *Dev Cell* **22**: 446–458.

D'Angelo MA, Raices M, Panowski SH, Hetzer MW. 2009. Age-Dependent Deterioration of Nuclear Pore Complexes Causes a Loss of Nuclear Integrity in Postmitotic Cells. *Cell* **136**: 284–295.

Di Micco R, Sulli G, Dobreva M, Liontos M, Botrugno OA, Gargiulo G, dal Zuffo R, Matti V, d'Ario G, Montani E, et al. 2011. Interplay between oncogene-induced DNA damage response and heterochromatin in senescence and cancer. *Nat Cell Biol* **13**: 292-302.

Doucet CM, Talamas JA, Hetzer MW. 2010. Cell cycle-dependent differences in nuclear pore complex assembly in metazoa. *Cell* **141**: 1030–1041.

Dultz E, Ellenberg J. 2010. Live imaging of single nuclear pores reveals unique assembly kinetics and mechanism in interphase. *J Cell Biol* **191**: 15-22.

Frosst P, Guan T, Subauste C, Hahn K, Gerace L. 2002. Tpr is localized within the nuclear basket of the pore complex and has a role in nuclear protein export. *J Cell Biol* **156**: 617–630.

Funakoshi T, Clever M, Watanabe A, Imamoto N. 2011. Localization of Pom121 to the inner nuclear membrane is required for an early step of interphase nuclear pore complex assembly. *Mol Biol Cell* **22**: 1058–1069.

Garcia-Segura LM, Lafarga M, Berciano MT, Hernandez P, Andres MA. 1989. Distribution of nuclear pores and chromatin organization in neurons and glial cells of the rat cerebellar cortex. *J Comparative Neurol* **290**: 440–450.

Guelen L, Pagie L, Brasset E, Meuleman W, Faza MB, Talhout W, Eussen BH, de Klein A, Wessels L, de Laat W, et al. 2008. Domain organization of human chromosomes revealed by mapping of nuclear lamina interactions. *Nature* **453**: 948–951.

Hari P, Acosta JC. 2017. Detecting the Senescence-Associated Secretory Phenotype (SASP) by High Content Microscopy Analysis. In *Oncogene-Induced Senescence: Methods and Protocols* (ed. M.A. Nikiforov), pp. 99–109, Springer New York, New York, NY https://doi.org/10.1007/978-1-4939-6670-7_9.

Hase ME, Cordes VC. 2003. Direct Interaction with Nup153 Mediates Binding of Tpr to the Periphery of the Nuclear Pore Complex. *Mol Biol Cell* **14**: 1923–1940.

Hoelz A, Debler EW, Blobel G. 2011. The structure of the nuclear pore complex. Annu Rev Biochem. 2011;**80**: 613-643.

Kim SJ, Fernandez-Martinez J, Nudelman I, Shi Y, Zhang W, Raveh B, Herricks T, Slaughter BD, Hogan JA, Upla P, et al. 2018. Integrative structure and functional anatomy of a nuclear pore complex. *Nature* **555**: 475-482.

Kosar M, Bartkova J, Hubackova S, Hodny Z, Lukas J, Bartek J. 2011. Senescence-associated heterochromatin foci are dispensable for cellular senescence, occur in a cell type- and insult-dependent manner and follow expression of p16ink4a. *Cell Cycle* **10**: 457–468.

Krull S, Dörries J, Boysen B, Reidenbach S, Magnius L, Norder H, Thyberg J, Cordes VC. 2010. Protein Tpr is required for establishing nuclear pore-associated zones of heterochromatin exclusion. *EMBO J* **29**: 1659–1673.

Lelek M, Casartelli N, Pellin D, Rizzi E, Souque P, Severgnini M, Di Serio C, Fricke T, Diaz-Griffero F, Zimmer C, et al. 2015. Chromatin organization at the nuclear pore favours HIV replication. *Nat Comms* **6**: 6483.

Lenain C, de Graaf CA, Pagie L, Visser NL, de Haas M, de Vries SS, Peric-Hupkes D, van Steensel B, Peeper DS. 2017. Massive reshaping of genome–nuclear lamina interactions during oncogene-induced senescence. *Genome Res* **27**: 1634–1644.

Lukášová E, Kovarˇík A, Bacˇíková A, Falk M, Kozubek S. 2017. Loss of lamin B receptor is necessary to induce cellular senescence. *Biochem J* **474**: 281-300.

Maeshima K, Yahata K, Sasaki Y, Nakatomi R, Tachibana T, Hashikawa T, Imamoto F, Imamoto N. 2006. Cell-cycle-dependent dynamics of nuclear pores: pore-free islands and lamins. *J Cell Sci* **119**: 4442-4451.

McCloskey A, Ibarra A, Hetzer MW. 2018. Tpr regulates the total number of nuclear pore complexes per cell nucleus. Genes Dev. 32:1321-1331.

Narita M, Narita M, Krizhanovsky V, Nuñez S, Chicas A, Hearn SA, Myers MP, Lowe SW. 2006. A Novel Role for High-Mobility Group A Proteins in Cellular Senescence and Heterochromatin Formation. *Cell* **126**: 503–514.

Narita M, Nuñez S, Heard E, Narita M, Lin AW, Hearn SA, Spector DL, Hannon GJ, Lowe SW. 2003. Rb-Mediated Heterochromatin Formation and Silencing of E2F Target Genes during Cellular Senescence. *Cell* **113**: 703–716.

Raices M, D'Angelo MA. 2012. Nuclear pore complex composition: a new regulator of tissue-specific and developmental functions. *Nat Rev Mol Cell Biol* **13**: 687–699.

Rodriguez-Bravo V, Pippa R, Song W-M, Carceles-Cordon M, Dominguez-Andres A, Fujiwara N, Woo J, Koh AP, Ertel A, Lokareddy RK, et al. 2018. Nuclear Pores Promote Lethal Prostate Cancer by

316 Increasing POM121-Driven E2F1, MYC, and AR Nuclear Import. *Cell* **174**: 1200-1215.

317 Sadaie M, Salama R, Carroll T, Tomimatsu K, Chandra T, Young ARJ, Narita M, Pérez-Mancera PA,
318 Bennett DC, Chong H, et al. 2013. Redistribution of the Lamin B1 genomic binding profile affects
319 rearrangement of heterochromatic domains and SAHF formation during senescence. *Genes Dev* **27**:
320 1800–1808.

321 Schermelleh L, Carlton PM, Haase S, Shao L, Winoto L, Kner P, Burke B, Cardoso MC, Agard DA,
322 Gustafsson MGL, et al. 2008. Subdiffraction multicolor imaging of the nuclear periphery with 3D
323 structured illumination microscopy. *Science* **320**: 1332–1336.

324 Sellés J, Penrad-Mobayed M, Guillaume C, Fuger A, Auvray L, Faklaris O, Montel F. 2017. Nuclear
325 pore complex plasticity during developmental process as revealed by super-resolution microscopy.
326 *Scientific Reports* **7**: 14732.

327 Solovei I, Wang AS, Thanisch K, Schmidt CS, Krebs S, Zwerger M, Cohen TV, Devys D, Foisner R,
328 Peichl L, et al. 2013. LBR and lamin A/C sequentially tether peripheral heterochromatin and inversely
329 regulate differentiation. *Cell* **152**: 584–598.

330 Zhang R, Chen W, Adams PD. 2007. Molecular Dissection of Formation of Senescence-Associated
331 Heterochromatin Foci. *Mol Cell Biol* **27**: 2343–2358.

332 Zhang R, Poustovoitov MV, Ye X, Santos HA, Chen W, Daganzo SM, Erzberger JP, Serebriiskii IG,
333 Canutescu AA, Dunbrack RL, et al. 2005. Formation of MacroH2A-Containing Senescence-Associated
334 Heterochromatin Foci and Senescence Driven by ASF1a and HIRA. *Dev Cell* **8**: 19–30.

335

336 **Figure Legends**

337 **Figure 1. Nuclear pore density increases in OIS**

338 A) Model of the nuclear pore complex showing the position of TPR, NUP153 and POM121. Adapted
339 from (Hoelz et al. 2011).

340 B) Schematic showing the balance of forces attracting heterochromatin to the nuclear lamina and
341 repelling heterochromatin from nuclear pores.

342 C) Schematic of OIS induction in ER:Ras cells by 4HT and continued proliferation in ER:Stop cells.

343 D) Western blot showing POM121 (left panel) and TPR (right panel) levels in 4HT treated ER:Stop and
344 ER:Ras cells.

345 E) TPR immunostaining in ER:STOP and ER:Ras cells treated with 4HT. Left: bottom plane of nucleus
346 imaged by SIM. Right: enlargement of the insets. Scale bars 2μm.

347 F) Mean (+/- SEM) nuclear pore density (pores/μm^2) in 4HT treated ER:Stop and ER:Ras cells as
348 counted by TPR staining in 3 biological replicates, ***p=0.0001.

349 G) As for F) but for Pom121 staining. h.s = highly significant p=$1.3E^{-06}$.

Figure 2. Increased nuclear pore density in OIS is necessary for SAHF formation

A) Schematic showing depletion experiment for panels B to E.

B) MAB414 (antibody recognizing several nucleoporins) immunostaining in ER:STOP cells treated with 4HT after 2 days knockdown with scramble (Scr) or POM121 siRNAs. Left: bottom plane of nucleus imaged by SIM. Right: enlargement of the insets. Scale bars 2μm.

C) Mean (+/- SEM) nuclear pore density (pores/μm^2) in 4HT treated ER:Stop cells after scramble (Scr) or POM121 siRNA knockdown, as assayed by TPR staining in 3 biological replicates, * $p<0.05$.

D) DAPI staining of 4HT-treated ER:Stop and ER:Ras cells in controls (Scr) and upon POM121 depletion (siPOM121). Scale bars 10μm. Bottom: enlargement of the insets.

E) Mean (+/- SEM) % of cells containing SAHF in 4HT-treated ER:Stop and ER:Ras cells after knockdown with scramble (Scr) siRNAs and in 4HT-treated ER:Ras cells with POM121 siRNAs. Data from 3 experiments. *$p<0.05$, h.s=highly significant.

Figure 3. TPR is necessary for SAHF formation and maintenance

A) DAPI staining of non-senescent 4HT treated ER:Stop and OIS (ER:Ras) cells after control scramble (Scr) siRNA and upon TPR depletion (siTPR). Scale bars 10μm.

B) Mean (+/- SEM) % of cells containing SAHF in 4HT-treated ER:Stop and ER:Ras cells after knockdown siRNAs as in (A). Data from 3 experiments. **$p<0.01$, h.s=highly significant.

C) Time course for TPR depletion by siRNA late in the OIS programme as performed for panels D-F.

D) DAPI staining of 4HT-treated ER:STOP and OIS cells ER:Ras in controls (Scr) and upon TPR depletion (siTPR). Scale bars 2μm.

E) Mean (+/- SEM) % of cells containing SAHF in 4HT-treated ER:Stop and ER:Ras cells after knockdown with scramble (Scr) siRNAs and in ER:Ras cells with TPR siRNAs. Data from 3 experiments. **$p<0.01$, h.s=highly significant.

F) DAPI (blue) and TPR (red) staining of 4HT-treated ER:STOP and ER:Ras upon TPR depletion (siTPR) imaged by SIM. Right: enlargement of the insets. Scale bars 2μm.

G) DAPI (blue) and TPR (red) staining of 4HT-treated ER:Ras cells upon TPR depletion (top). Bottom image shows co-staining with the nucleoporin antibody MAB414 (green).

Figure 4. TPR is necessary for the SASP

A) Mean (± SEM) mRNA level, measured by qRT-PCR for SASP genes (*IL1α, IL1β, IL6,I L8*), in 4HT-treated ER:Stop and ER:Ras cells after knockdown with scramble (Scr) siRNAs and in 4HT-treated ER:Ras cells with TPR siRNAs. Expression is relative to ER:Ras cells transfected with Scr siRNAs. Data from 3 experiments. h.s=highly significant.

B) Mean (± SEM) % of cells positive by immunostaining for SASP cytokines (IL1α, IL1β, IL6,IL8) in 4HT-treated ER:Stop and ER:Ras cells after SiRNA knockdown as in (A). Data from 3 experiments. **p<0.01, *** p<0.001, h.s=highly significant.

C) Immunostaining (green) for IL1α and IL1β in DAPI (blue) stained nuclei of 4HT-treated ER:Stop and ER:Ras cells subjected to RNAi as in (A). Scale bars 100μm.

Figure 5. Chromatin reorganization seems necessary for the SASP

A) Mean (± SEM) ASF1a mRNA level, established by qRT-PCR, in 4HT-treated ER:STOP and ER:Ras cells after knockdown with scramble (Scr) or ASF1a siRNAs. Expression is shown relative to ER:STOP cells transfected with Scr siRNAs. Data from 3 experiments. *p<0.05.

B) DAPI staining of 4HT-treated ER:STOP and ER:Ras cells in controls (Scr) and upon ASF1a depletion (siASF1a). Scale bars 2μm

C) Mean (+/- SEM) % of cells containing SAHF in 4HT-treated ER:Stop and ER:Ras cells after knockdown with scramble (Scr) siRNAs and in ER:Ras cells with ASF1a SiRNAs. Data from 3 experiments. ***p<0.001.

D) Mean (+/- SEM) nuclear pore density (pores/μm^2) in 4HT treated ER:Stop cells after knock down with scramble (Scr) or ASF1a (siASF1a) siRNAs as counted by MAB414 or TPR staining in 3 biological replicates, n.s= non significant.

E) Mean (± SEM) mRNA levels, measured by qRT-PCR for *IL1α*, *IL1β*, *IL6*, *IL8*, in 4HT-treated ER:Stop and ER:Ras cells after knockdown with scramble (Scr) siRNAs and in 4HT-treated ER:Ras cells with ASF1a siRNAs. Expression is shown relative to ER:Ras cells transfected with Scr siRNAs. Data from 3 experiments. ***p<0.001, h.s=highly significant.

Acknowledgments

C.B. was supported by a H2020 Marie-Curie IF (655350 – NPCChr) and a Bettencourt-Schueller foundation prize for young researchers . JCA is supported by a Career Development Fellowship from Cancer Research UK. W.A.B is supported by a Medical Research Council (MRC) University Unit grant MC_PC_U127527202. We thank the Edinburgh Super-Resolution Imaging Consortium and IGMM Advanced Imaging Resource for assistance with imaging and Robert Illingworth (MRC HGU, Edinburgh) for the Volcano plot of mRNA expression.

Authors contribution

CB and WAB conceived the experiments and designed the experiments together with JCA. P.H performed qRT-PCRs and immunostaining for cytokines of the SASP and siRNA transfections for many of the experiments. CB conducted most of the other experiments including; super-resolution microscopy, counting of nuclear pore densities and identification of cells containing SAHFs. KCFO assisted with immunoblotting. CB and WAB wrote the manuscript with input from all authors.

Competing interests: The authors declare that they have no competing interests.

Materials and correspondence: Correspondence and material requests should be addressed to WAB

Figure 1. Boumendil

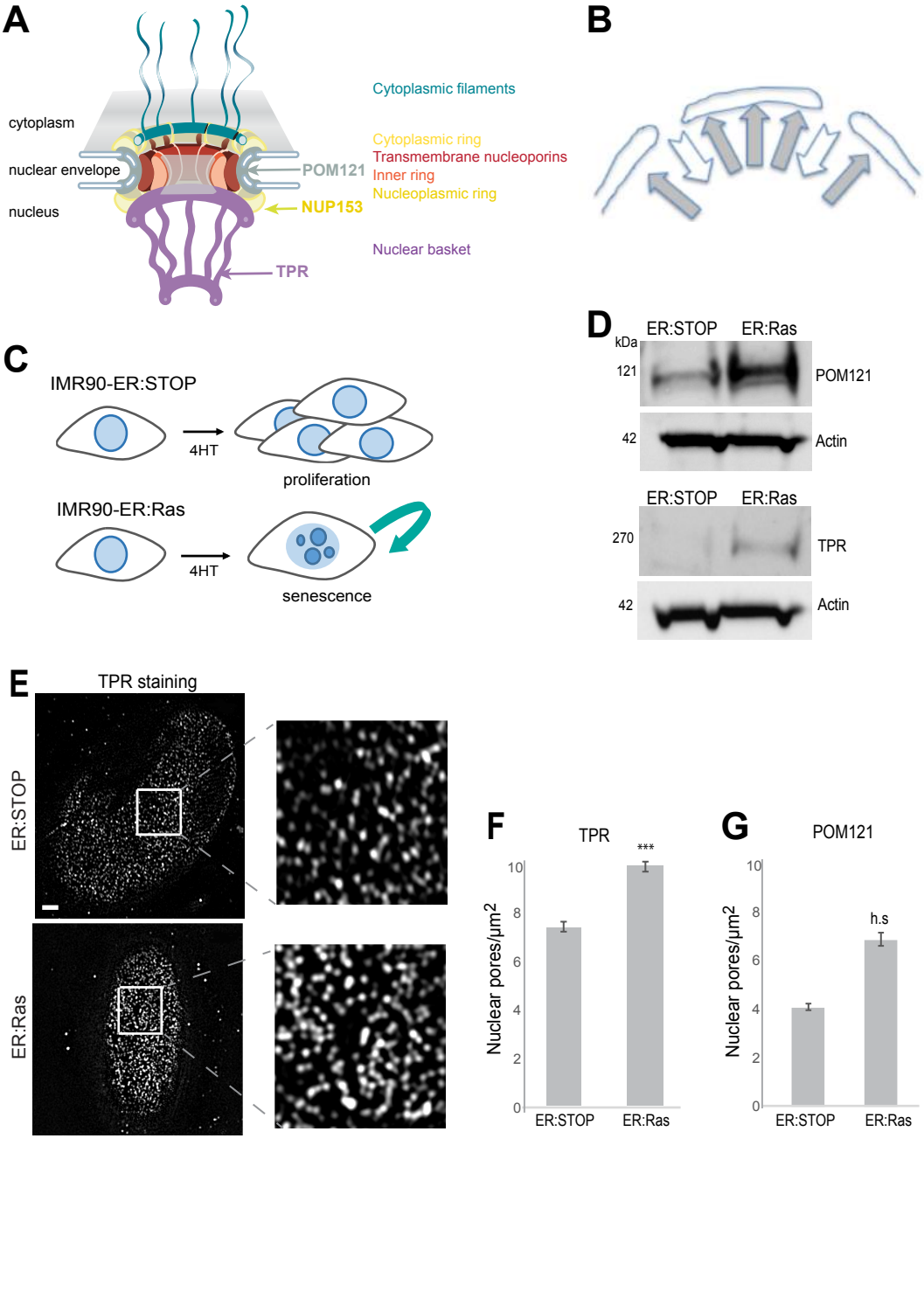

Figure 2. Boumendil

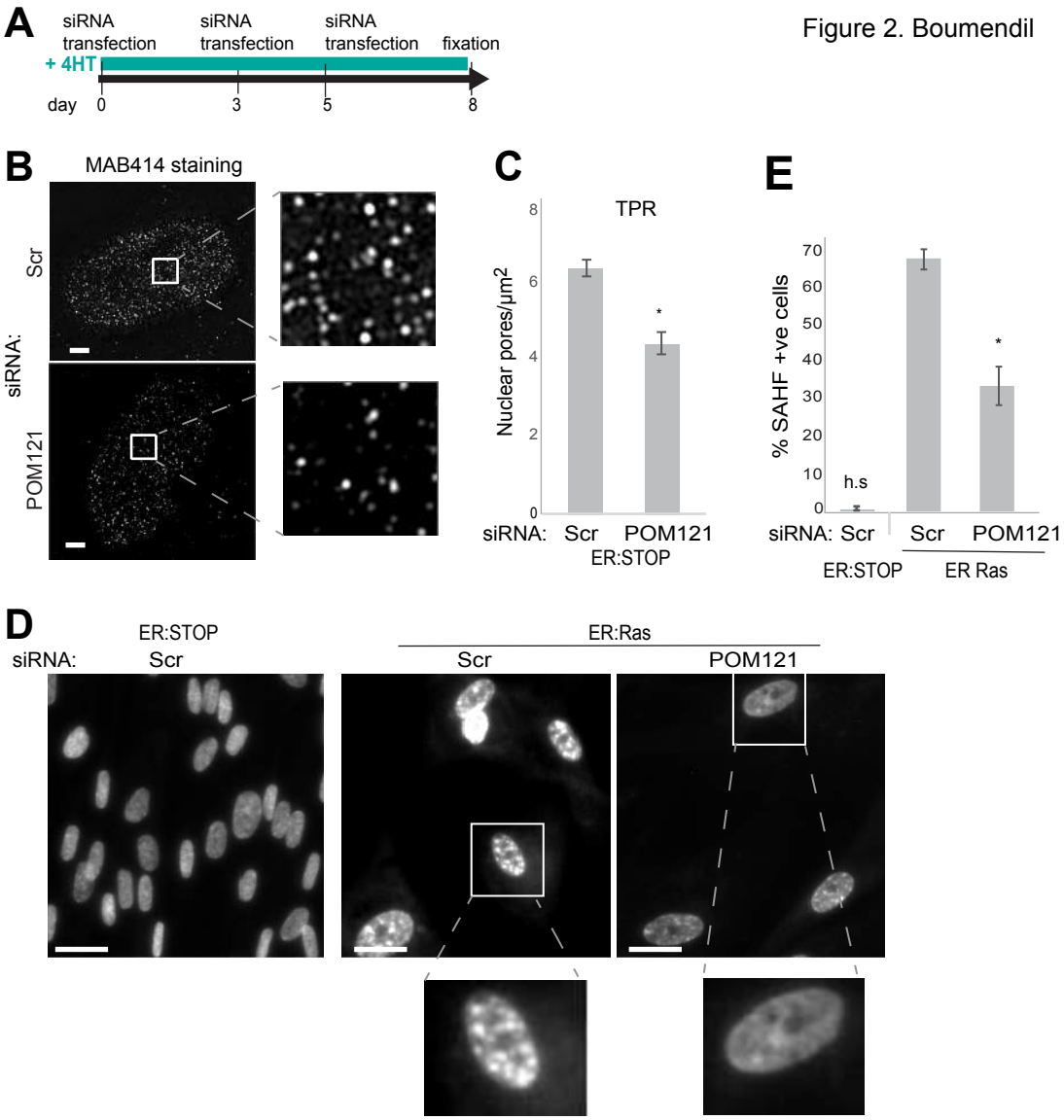

Figure 3 - Boumendil

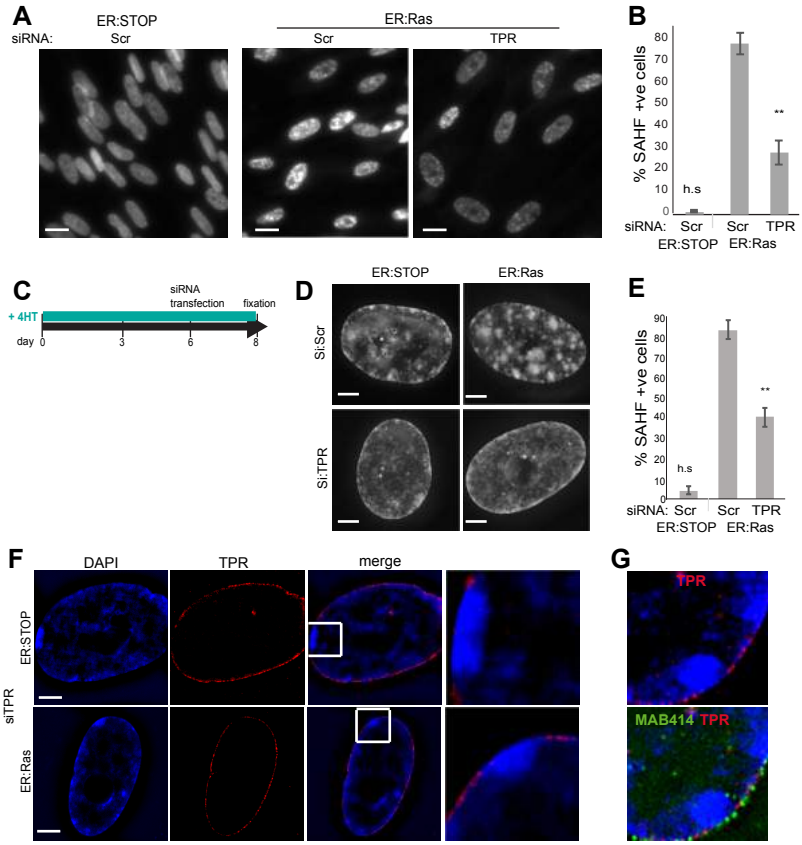

Figure 4. Boumendil

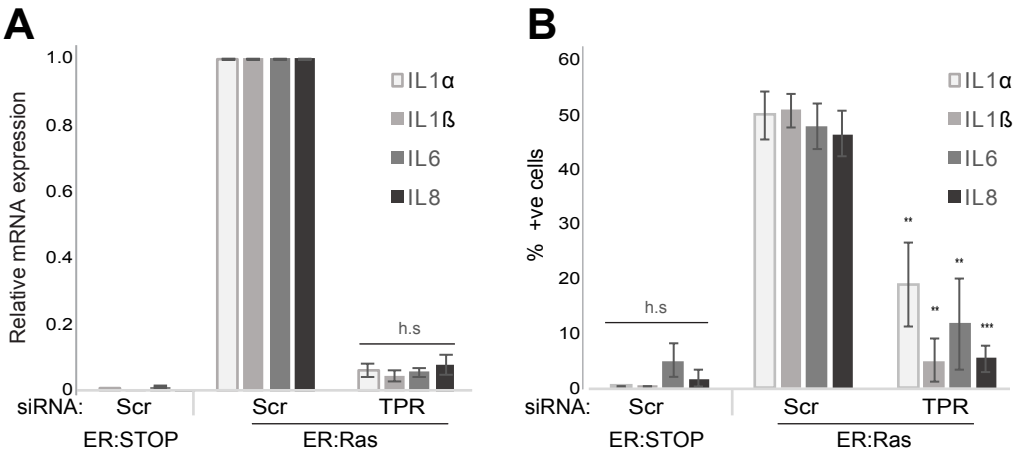

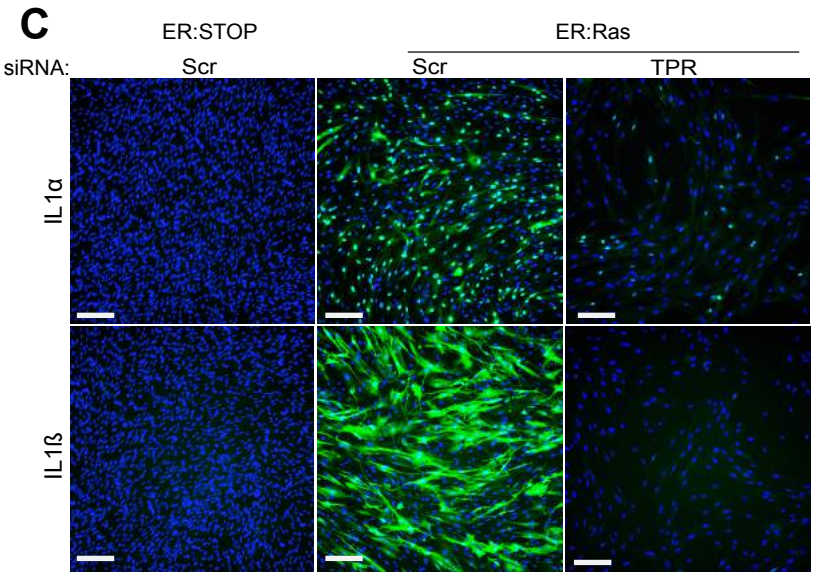

Figure 5. Boumendil